Cysteinyl leukotrienes and acetylcholine are biliary tuft cell cotransmitters

Maryam Keshavarz[1,2], Schayan Faraj Tabrizi[1,2], Anna-Lena Ruppert[3], Uwe Pfeil[1,2], Yannick Schreiber[4], Jochen Klein[5], Isabell Brandenburger[2,6], Günter Lochnit[7], Sudhanshu Bhushan[8], Alexander Perniss[1,2], Klaus Deckmann[1,2], Petra Hartmann[1,2], Mirjam Meiners[1,2], Petra Mermer[1,2], Amir Rafiq[1,2], Sarah Winterberg[3], Tamara Papadakis[1,2], Dominique Thomas[9,10], Carlo Angioni[9], Johannes Oberwinkler[11], Vladimir Chubanov[12], Thomas Gudermann[12], Ulrich Gärtner[1], Stefan Offermanns[2,6], Burkhard Schütz[3]*, Wolfgang Kummer[1,2]*

The gallbladder stores bile between meals and empties into the duodenum upon demand and is thereby exposed to the intestinal microbiome. This exposure raises the need for antimicrobial factors, among them, mucins produced by cholangiocytes, the dominant epithelial cell type in the gallbladder. The role of the much less frequent biliary tuft cells is still unknown. We here show that propionate, a major metabolite of intestinal bacteria, activates tuft cells via the short-chain free fatty acid receptor 2 and downstream signaling involving the cation channel transient receptor potential cation channel subfamily M member 5. This results in corelease of acetylcholine and cysteinyl leukotrienes from tuft cells and evokes synergistic paracrine effects upon the epithelium and the gallbladder smooth muscle, respectively. Acetylcholine triggers mucin release from cholangiocytes, an epithelial defense mechanism, through the muscarinic acetylcholine receptor M3. Cysteinyl leukotrienes cause gallbladder contraction through their cognate receptor CysLTR1, prompting emptying and closing. Our results establish gallbladder tuft cells as sensors of the microbial metabolite propionate, initiating dichotomous innate defense mechanisms through simultaneous release of acetylcholine and cysteinyl leukotrienes.

INTRODUCTION

In most vertebrates, the gallbladder serves as a reservoir to store the constantly produced bile arriving from the liver between meals. It is lined by a simple mucosa consisting of (i) an abundant columnar cell type, the cholangiocyte, serving all currently known epithelial functions such as electrolyte transport, water reabsorption, and mucin production (*1*), and (ii) infrequent tuft or brush cells, characterized by distinct microvilli, but with unknown function (*2*, *3*). These biliary tuft cells express the cation channel transient receptor potential cation channel subfamily M member 5 (TRPM5), characteristic for specialized sensory cells (*4*), and the acetylcholine (ACh)–synthesizing enzyme, choline acetyltransferase (ChAT) (*5*). Solitary cells with a similar signature at other locations are considered as sentinels monitoring the luminal content for microbial products, triggering cholinergic neural avoidance reflexes or local type 2 immune reactions upon stimulation, respectively (*6*–*8*). Absence of these cells or a defective signal transduction due to TRPM5 deficiency results in higher susceptibility to airway infection and impaired worm clearance from the intestine (*9*–*11*). In view of the exposure of the gallbladder to the intestinal microbiome through its connection to the duodenum, we hypothesized that gallbladder tuft cells may serve similar innate immune functions. We considered ACh as a primary mediator, because tuft cells express the ACh-synthesizing enzyme and tuft cell–derived ACh triggers innate defense mechanisms in the airways (*11*, *12*). The activating stimuli for gallbladder tuft cells have not yet been determined. Thus, we first chose an optogenetic model that we recently validated on airway tuft cells (*11*) to stimulate gallbladder tuft cells directly, which allowed us to elucidate their effector mechanisms. We then used these readouts and genetic models to identify a naturally occurring intestinal microbial product as a tuft cell activator.

RESULTS

Tuft cell ACh evokes mucin release

We used optogenetic mice expressing the light-sensitive channel channelrhodopsin-2 (ChR2) under the control of the ChAT promoter. In bacterial artificial chromosome (BAC) transgenic ChAT-ChR2-EYFP (enhanced yellow fluorescent protein) mice (*13*), the ChR2-EYFP fusion protein was expressed in and targeted to the cell membrane of gallbladder tuft cells, identified by immunolabeling with antibodies against ChAT, PLCβ2 (the phospholipase C isoform characteristic for chemosensory cells), TRPM5, and Pou2f3 (transcription factor essential for tuft cell development) (fig. S1) (*14*), but not in nerve fibers (fig. S2). Light-emitting diode (LED) illumination of explanted gallbladders of this strain, but not of controls, resulted in an increase in the ACh concentration in the supernatant (Fig. 1A). On the basis of early studies with cholinergic agonists (*15*), which we replicated

[1]Institute of Anatomy and Cell Biology, German Center for Lung Research, Justus Liebig University Giessen, Giessen, Germany. [2]Excellence Cluster Cardio-Pulmonary Institute, Justus Liebig University Giessen, Giessen, Germany. [3]Institute of Anatomy and Cell Biology, Philipps University, Marburg, Germany. [4]Fraunhofer Institute for Molecular Biology and Applied Ecology IME, Project Group TMP, Frankfurt, Germany. [5]Department of Pharmacology and Clinical Pharmacy, College of Pharmacy, Goethe University Frankfurt, Frankfurt, Germany. [6]Department of Pharmacology, Max Planck Institute for Heart and Lung Research, Bad Nauheim, Germany. [7]Institute of Biochemistry, Justus Liebig University Giessen, Giessen, Germany. [8]Institute of Anatomy and Cell Biology, Unit of Reproductive Biology, Justus Liebig University Giessen, Giessen, Germany. [9]Pharmazentrum Frankfurt/ZAFES, Institute of Clinical Pharmacology, Goethe University Frankfurt, Frankfurt, Germany. [10]Fraunhofer Institute for Translational Medicine and Pharmacology ITMP, Frankfurt, Germany. [11]Philipps-Universität Marburg, Institut für Physiologie und Pathophysiologie, Marburg, Germany. [12]Walther Straub Institute of Pharmacology and Toxicology, German Center for Lung Research, Ludwig-Maximilians-Universität München, Munich, Germany.
*Corresponding author. Email: wolfgang.kummer@anatomie.med.uni-giessen.de (W.K.); schuetzb@staff.uni-marburg.de (B.S.)

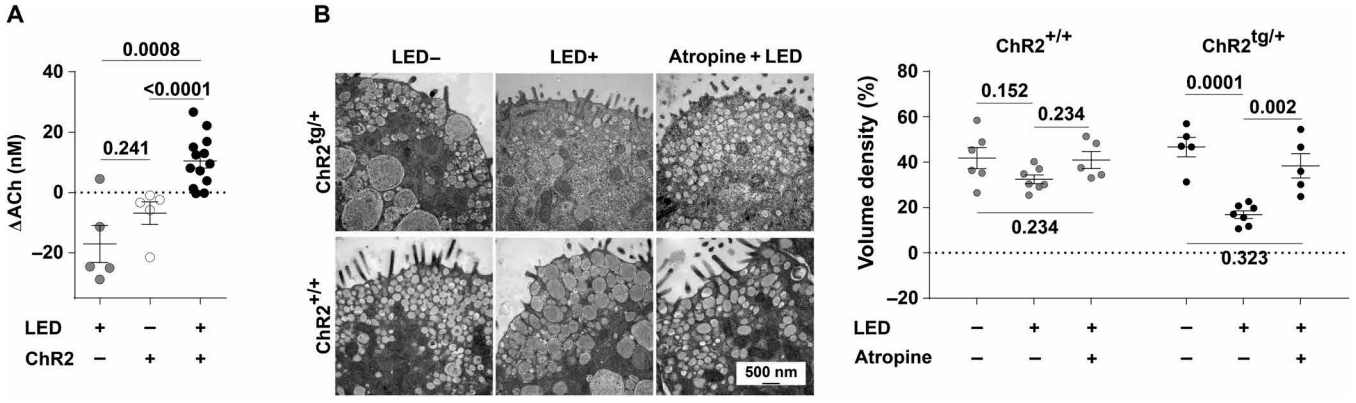

Fig. 1. Tuft cell ACh evokes mucin release. (**A**) ACh release (stimulated minus values before stimulation) into supernatant in response to LED illumination (LED+) of explanted gallbladders from ChAT-ChR2-EYFP ($ChR2^+$, $n = 13$) and from C57BL/6 ($ChR2^-$, $n = 5$) mice. Non–LED illuminated (LED–) $ChR2^+$ mice ($n = 5$) served as control. (**B**) Mucin granule volume density measurements in the apical cytoplasm of cholangiocytes of explanted ChAT-ChR2-EYFP ($ChR2^{tg/+}$) and C57BL/6 ($ChR2^{+/+}$) gallbladders with (LED+) and without (LED–) illumination, in the presence (+) or absence (–) of the muscarinic blocker atropine ($n = 5$ to 7 for all groups). Representative ultrastructural images are shown on the left. ANOVA with Tukey post hoc correction. Validation of ChR2 mouse model shown in figs. S1 and S2.

for validation (fig. S3), we reasoned that this tuft cell–derived ACh may cause glycoprotein secretion from neighboring cholangiocytes. Ultrastructural volume density of mucin granules, an established stereological parameter for induced glycoprotein secretion from cholangiocytes (*15*), dropped by 65% upon 3 min of LED illumination in ChAT-ChR2-EYFP gallbladders but not in corresponding wild-type gallbladders. This effect was caused by ACh because it was sensitive to the muscarinic ACh receptor inhibitor atropine (Fig. 1B).

Tuft cell CysLTs evoke contraction

Besides epithelial effects, ACh also causes gallbladder contraction mediated by the M3 muscarinic receptor (M3R) (fig. S4, A and B) (*16*). Thus, we further tested the impact of tuft cell stimulation on gallbladder smooth muscle tension in an organ bath approach. Optogenetic stimulation of explanted ChAT-ChR2-EYFP gallbladders induced a sharp increase in tension followed by a plateau phase after cessation of the stimulus (fig. S4C). We also used another mouse strain expressing a ChR2-tdTomato fusion protein induced by Cre recombinase expression driven by the endogenous ChAT promoter. In contrast to the expression pattern seen in ChAT-ChR2-EYFP mice, the ChR2-tdTomato fusion protein was expressed in cholinergic nerve fibers but not in tuft cells (fig. S5). LED illumination of gallbladders from these ChAT-ChR2-tdTomato mice evoked no contraction (fig. S4C), corroborating earlier reports that nerve stimulation does not evoke cholinergic contraction in the mouse gallbladder (*17*). In LED-illuminated ChAT-ChR2-EYFP gallbladders, neither the peak response nor the plateau was sensitive to the muscarinic blocker atropine, except when enzymatic ACh breakdown was prevented by the cholinesterase inhibitor eserine (fig. S4, C to E). This suggested spatial restriction of ACh effects by endogenous presence of cholinesterases, consistent with specific acetylcholinesterase (AChE) activity in a plexus of mucosal and muscular nerve fibers and, less prominently, butyrylcholinesterase (BChE) activity in the epithelium (fig. S4, F and G). Together, these data showed that tuft cells release another contractor compound, distinct from ACh.

Besides ACh, arachidonic acid–derived prostaglandins and leukotrienes are potent gallbladder constrictors (*18*), and respiratory and intestinal tuft cells express their synthesizing enzymes and release cysteinyl leukotrienes (CysLTs) (*5*, *9*, *19*–*21*). We here identified both prostaglandin-synthesizing cyclooxygenases (COX1 and COX2) and arachidonate 5-lipoxygenase (ALOX5), its activating protein (5-lipoxygenase-activating protein or FLAP), and leukotriene C4 synthase (LTC4S), the enzyme-generating CysLTs (LTC_4, LTD_4, and LTE_4) from LTA_4, in cholinergic tuft cells of the mouse gallbladder (Fig. 2, A to D, and figs. S6 and S7). FLAP was not restricted to tuft cells but also seen in some cells of the subepithelial lamina propria (Fig. 2B), consistent with its reported occurrence in leukocytes (*22*). These data showed that gallbladder tuft cells are equipped with the enzymatic machineries to generate both prostaglandins and CysLTs.

Optogenetic activation of tuft cells in explanted gallbladders from ChAT-ChR2-EYFP mice resulted in a significant decrease in prostaglandin D2 and the stable prostaglandin metabolite 6-keto-prostaglandin $F_{1\alpha}$ in the supernatant, concomitant with increased levels of CysLTs (Fig. 2, D to F). All three CysLTs contracted explanted gallbladders with a rank order of potency of $LTC_4 > LTD_4 > LTE_4$ (fig. S8, A to C). This profile suggested action through CysLT receptor 1 or 2 (CysLTR1 or CysLTR2) (*23*), both of which were found to be expressed in the gallbladder (fig. S8D). When given in the plateau phase of contraction after a first LED stimulus in the optogenetic approach, the CysLTR1 inhibitor MK-571 (fig. S8, A and B) brought tension back to baseline. Thereafter, the gallbladder responded only minimally to a subsequent second LED illumination, whereas the response to the control stimulus cholecystokinin (CCK) remained undiminished (Fig. 2G). These data provided evidence for CysLT release from activated tuft cells, causing gallbladder contraction via their cognate receptor CysLTR1.

Propionate triggers tuft cell CysLT signaling to muscle

Guided by the hypothesis that gallbladder tuft cells serve as sentinels monitoring the luminal content for ascending material from the gut through the bile duct, we considered metabolites of the intestinal microbiome as naturally occurring tuft cell activators. Fermentation of dietary nondigestible carbohydrates by gut microbiota yields high concentrations of the short-chain fatty acids (SCFAs) acetate, propionate, and butyrate (*24*), which exert multiple effects in the host through free fatty acid receptors 2 and 3 [FFAR2 and FFAR3, synonyms: G protein-coupled receptor (GPR)43 and GPR41] (*25*, *26*).

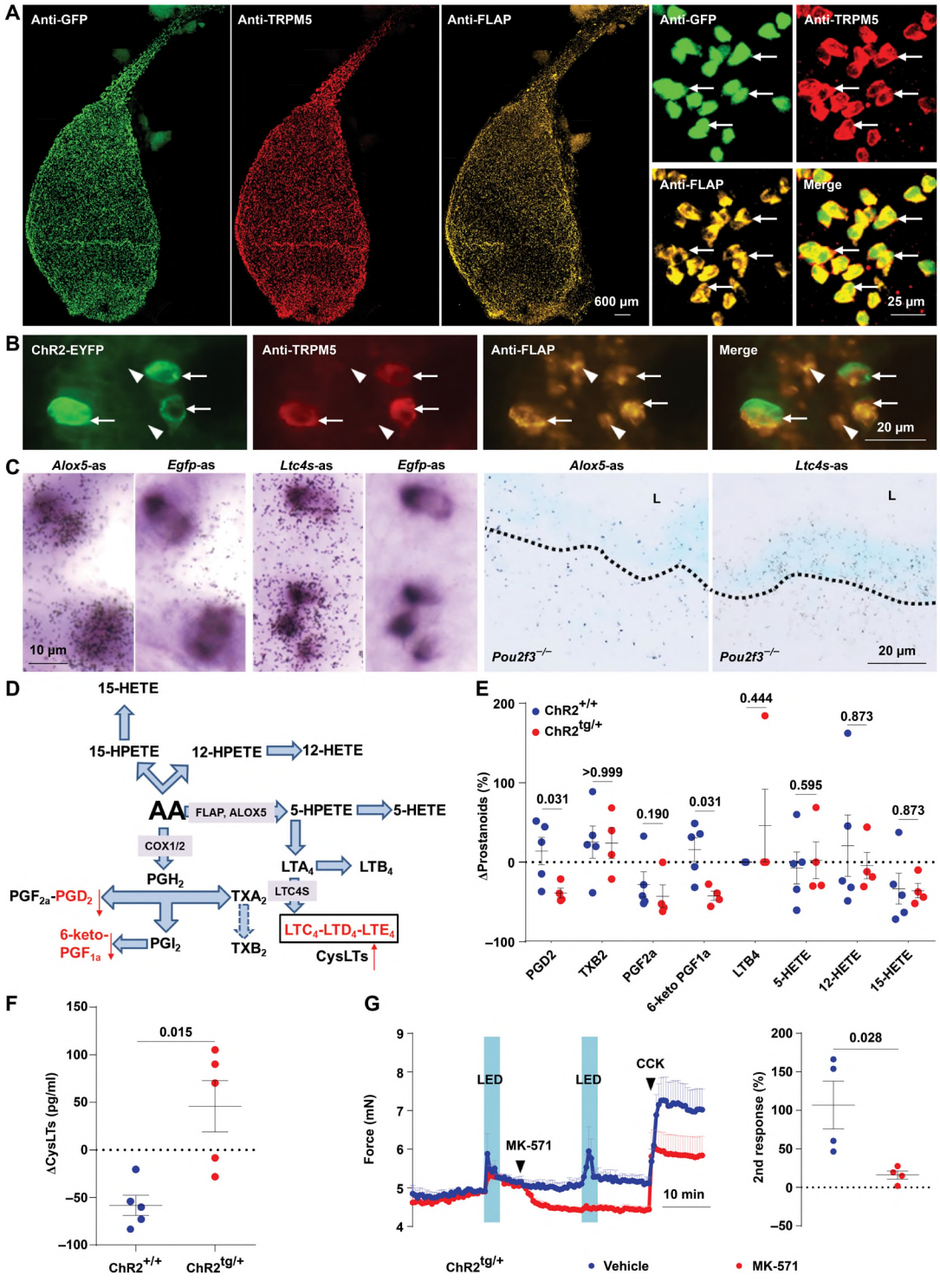

Fig. 2. Tuft cell CysLTs evoke contraction. (**A**) Triple immunofluorescence (anti-FLAP, anti-GFP, and anti-TRPM5) of cleared gallbladder. Arrows point to select cells that display all three labels (representative of $n = 3$). (**B**) Native ChR2-EYFP fluorescence in combination with anti-TRPM5 and anti-FLAP antibodies in gallbladder tissue section. Arrows point to epithelial cells that display all three labels; arrowheads point to subepithelial cells (representative of $n = 4$). (**C**) Double-labeling in situ hybridization with *Egfp*-antisense (as) (digoxigenin label, brownish) and *Alox5*-as and *Ltc4s*-as (radioactive label, black grains), respectively, in ChAT-EGFP gallbladders (first four panels; representative of $n = 4$ to 6 each). Single-labeling in situ hybridization with *Alox5*-as and *Ltc4s*-as (both radioactive label) in *Pou2f3*$^{-/-}$ gallbladders lacking tuft cells (last two panels; representative of $n = 4$ to 6 each). Epithelium lies above the dashed line; L, lumen. Controls: see fig. S7B. (**D**) Pathways of prostaglandin (PG) and leukotriene (LT) synthesis from arachidonic acid (AA), indicating key enzymes (gray boxes) detected in gallbladder tuft cells [see (A) to (C) and figs. S6 and S7], and expression changes in their products (red arrows) upon tuft cell activation [see (E) and (F)]. HPETE, hydroperoxyeicosatetraenoic acid; TX, thromboxane. (**E**) Changes in prostanoid release (Δ: stimulated minus values before stimulation, shown in percentage) after LED illumination of non–ChR2-expressing (ChR2$^{+/+}$) ($n = 5$) and ChR2-expressing (ChR2$^{tg/+}$) ($n = 4$) gallbladders. (**F**) Changes in CysLT release (Δ: stimulated minus values before stimulation, shown in picograms per milliliter) from ChR2$^{+/+}$ and ChR2$^{tg/+}$ gallbladders ($n = 5$ each). (**G**) Force recordings from ChR2$^{tg/+}$ gallbladders stimulated with LED in the presence (red line) and absence (blue line) of the CysLTR1 blocker, MK-571 (1 µM). Response to CCK serves as viability control ($n = 4$ for all). Scatterplot: maximum peak responses of the second stimulation (first response set as 100%) in the absence (vehicle, blue dots) and presence (red dots) of MK-571. Whiskers: means ± SEM throughout. Data are from three independent experiments in (E) to (G); Mann-Whitney test throughout.

Acetate, the SCFA with the highest concentrations in the gut (*27*), duodenal juice, and bile (Fig. 3A), acted as a weak contractor (fig. S9A). Butyrate had no effect on gallbladder tone at up to 10 mM (Fig. 3B), whereas propionate caused a rapid increase in muscle tension at concentrations up to 10 mM [median effective concentration (EC_{50}) = 0.24 mM] and a relaxation at 25 mM (Fig. 3C and fig. S9B). The actual propionate concentrations in bile (0.155 ± 0.044 mM) and duodenal juice (0.094 ± 0.016 mM) (Fig. 3A) were just below the effective range to evoke contraction. Propionate-induced contraction, but not that induced by LTD_4, was mediated by tuft cells,

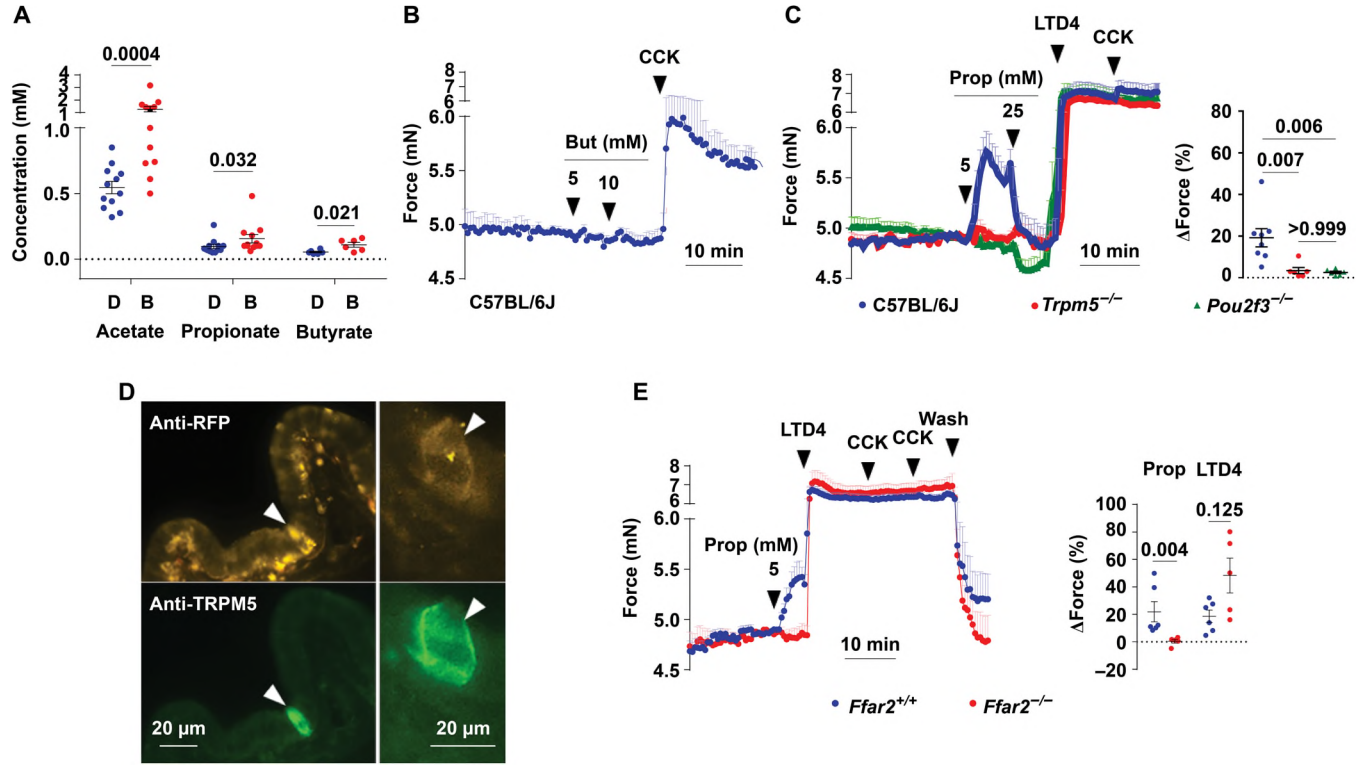

Fig. 3. Propionate triggers tuft cell to muscle signaling via FFAR2. (**A**) Concentrations of SCFAs in duodenal juice (D) and bile (B) ($n = 12$ for acetate and propionate and $n = 6$ for butyrate). (**B**) Force recordings of explanted C57BL/6J gallbladders ($n = 4$) exposed to 5 and 10 mM butyrate (But). Stimulation with CCK (0.1 µM) served as viability control. (**C**) Force recordings of explanted gallbladders from C57BL/6J, *Trpm5*$^{-/-}$, and *Pou2f3*$^{-/-}$ mice exposed to 5 and 25 mM propionate (Prop). Stimulation with LTD4 (0.1 µM) and CCK (0.1 µM) served as viability controls. (**D**) Double-labeling immunofluorescence with anti-RFP and anti-TRPM5 antibodies of gallbladder section of an FFAR2-RFP reporter mouse (representative images of $n = 3$). Arrowheads depict double-labeled epithelial cells. (**E**) Force recordings of explanted gallbladders taken from *Ffar2*$^{+/+}$ ($n = 6$) and from *Ffar2*$^{-/-}$ ($n = 5$) mice stimulated with propionate (5 mM). LTD4 (0.1 µM) and CCK (0.1 µM) served as viability controls. Scatterplots in (C) und (E) depict maximum responses. Whiskers: means ± SEM throughout. Data are from two independent experiments in (A) and (B), from five independent experiments in (C), and from three independent experiments in (E). Mann-Whitney test in (A) and (E); Kruskal-Wallis test followed by Dunn's multiple comparison test in (C).

because it was lost in tuft cell–deficient *Pou2f3*$^{-/-}$ mice (Fig. 3C), which still showed regular immune cell composition and expression of neutrophil and mast cell markers (fig. S10). Furthermore, propionate-induced contraction required the cation channel TRPM5 (Fig. 3C), which is restricted to tuft cells in the gallbladder (fig. S7C). FFAR2-RFP (red fluorescent protein) was expressed in TRPM5-positive gallbladder tuft cells (Fig. 3D), and the contractor response to propionate was selectively lost in gallbladders from *Ffar2* gene–deficient mice (Fig. 3E). Succinate, a microbial metabolite activating intestinal tuft cells (*6*, *28*), had no effect on gallbladder tone (fig. S9C). Collectively, this set of data demonstrated that propionate activates gallbladder tuft cells through an FFAR2-TRPM5 signaling pathway to induce gallbladder contraction via paracrine mechanisms.

On the basis of the findings obtained in the optogenetic model, we hypothesized that CysLTs are the constrictor mediators released from tuft cells in response to propionate. Propionate (5 mM) evoked release of CysLTs from explanted gallbladders even stronger than that observed in the optogenetic experiments, and this was fully blocked by the 5-lipoxygenase inhibitor, zileuton (10 µM), validating the specificity of the enzyme-linked immunosorbent assay (ELISA) data (Fig. 4A). Thus, we tested the effects of inhibiting the CysLT synthetic pathway on propionate-induced contraction. Both the 5-lipoxygenase inhibitor, zileuton (10 µM), and the LTC_4S inhibitor, MK-886 (1 µM), reduced baseline tension of gallbladders and largely prevented propionate-induced gallbladder contraction, leaving direct gallbladder responses to LTD_4 intact (Fig. 4, B and C). As in the optogenetic experiments, CysLTs exerted their effect through CysLTR1, because the effects evoked by propionate and LTD_4/LTC_4 were nearly abolished by pretreatment with the CysLTR1 inhibitor, MK-571, and in *Cysltr1* gene–deficient mice (Fig. 4, C and D). The incremental residual response seen after CysLTR1 inhibition did not reflect a cholinergic component, because it persisted in experiments with coadministration of atropine (Fig. 4C). Direct activation of CysLTR2 with *N*-methyl-LTC4 (0.1 µM) also evoked gallbladder contraction, which was fully sensitive to the specific CysLTR2 blocker HAMI3379 (1 µM) (Fig. 4E). The propionate response, however, was entirely preserved after CysLTR2 inhibition and, thus, did not involve this pathway (Fig. 4E).

Propionate triggers cholinergic tuft cell signaling to cholangiocytes

As in the optogenetic experiments, tuft cell–derived ACh caused decreased mucin granule density in cholangiocytes upon stimulation with propionate, suggestive of mucin release. This effect was specifically lost in animals with tuft cell–specific (*Avil*^{Cre}) (*11*) deletion of the ACh-synthesizing enzyme, ChAT (Fig. 5A), and was abolished in mice harboring a constitutive knockout of the M3R (Fig. 5B). Consistent with these ultrastructural data, propionate triggered a

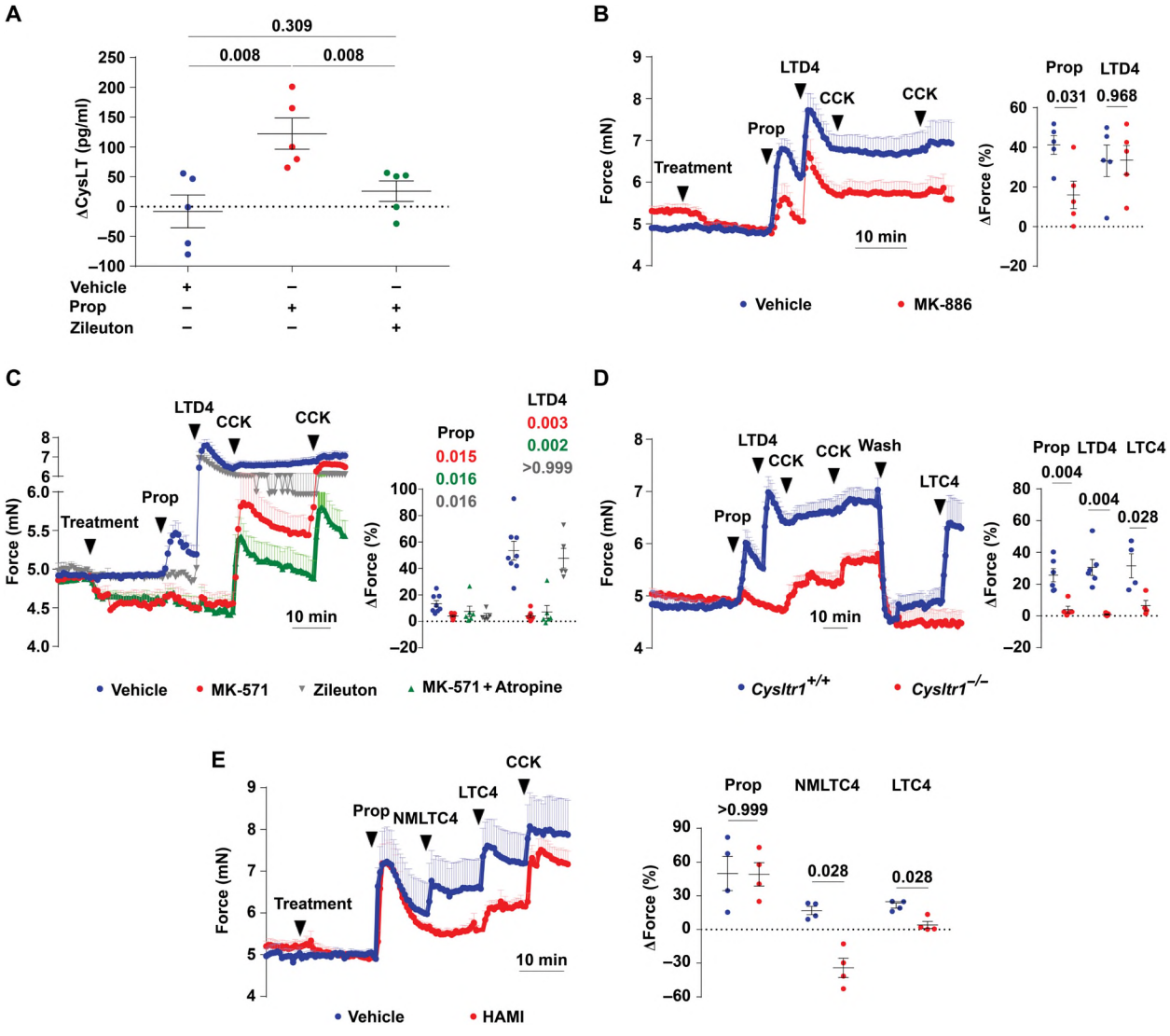

Fig. 4. Propionate triggers tuft cell CysLT signaling to muscle. (**A**) Measurements of CysLT release (Δ: stimulated minus values before stimulation, shown in picograms per milliliter) from C57BL/6J gallbladders ($n = 5$ each) upon stimulation with propionate (5 mM) and effect of the ALOX5 inhibitor zileuton (10 μM). (**B**) Effect of the FLAP inhibitor, MK-886 (1 μM), in comparison with vehicle on the response to stimulation with propionate (5 mM), LTD4 (0.1 μM), CCK (0.1 μM), and LTC4 (0.1 μM) in force recordings of explanted C57BL/6J gallbladders ($n = 5$ each). (**C**) Effects of zileuton (10 mM; $n = 5$), MK-571 (1 μM; $n = 7$), and MK-571 + atropine (1 μM) on the contractile response to propionate (5 mM), LTD4 (0.1 μM), and CCK (0.1 μM) in force recordings of explanted C57BL/6J gallbladders. (**D**) Force recordings of explanted gallbladders taken from *Cysltr1*$^{+/+}$ ($n = 6$) and from *Cysltr1*$^{-/-}$ ($n = 5$) mice stimulated with propionate (5 mM), LTD4 (0.1 μM), CCK (0.1 μM), and LTC4 (0.1 μM). (**E**) Force recordings of explanted C57BL/6J gallbladders; effect of pretreatment with the specific CysLTR2 inhibitor, HAMI (1 μM), on the responses evoked by propionate (5 mM), the CysLTR2 agonist *N*-methyl-LTC4 (NMLTC4; 0.1 μM), LTC4 (0.1 μM), and CCK (0.1 μM). Scatterplots in (B) to (E) depict maximum responses. Whiskers: means ± SEM throughout. Data are from three independent experiments in (A), (B), (D), and (E) and from five independent experiments in (C). Mann-Whitney test in (B), (D), and (E); Kruskal-Wallis test followed by Dunn's multiple comparison test in (A) and (C).

marked release of glycoprotein into the supernatant of stimulated gallbladders. This effect was dependent on the cation channel TRPM5 (Fig. 5C and fig. S11A) and, again, lost in animals with tuft cell–specific (*Avil*^{Cre}) deletion of ChAT (Fig. 5D and fig. S11B).

In the nose, solitary chemosensory cells—the nasal equivalent to tuft cells—exert effects through local reflex loops involving ACh release from chemosensory cells, activation of nicotinic receptors on nearby peptidergic, capsaicin-sensitive sensory nerve fibers, and neuropeptide (substance P) release from these terminals (*12*). Although contacts of gallbladder tuft cells to nerve fibers have not been noted by previous ultrastructural studies (*2*, *29*), we considered the possibility that similar neural pathways might also operate in the gallbladder. However, whole-mount immunostaining with a general neural marker (anti-PGP9.5) revealed no relationship between nerve fibers and tuft cells (fig. S12, A and B), and direct activation of peptidergic sensory nerve fibers with capsaicin did not trigger glycoprotein release in explanted gallbladders (fig. S12C).

Last, we explored whether tuft cells might play a role in homeostatic mucin production. Consistent with an earlier report (*30*), we found prominent expression of mucin genes *Muc1*, *Muc3*, and

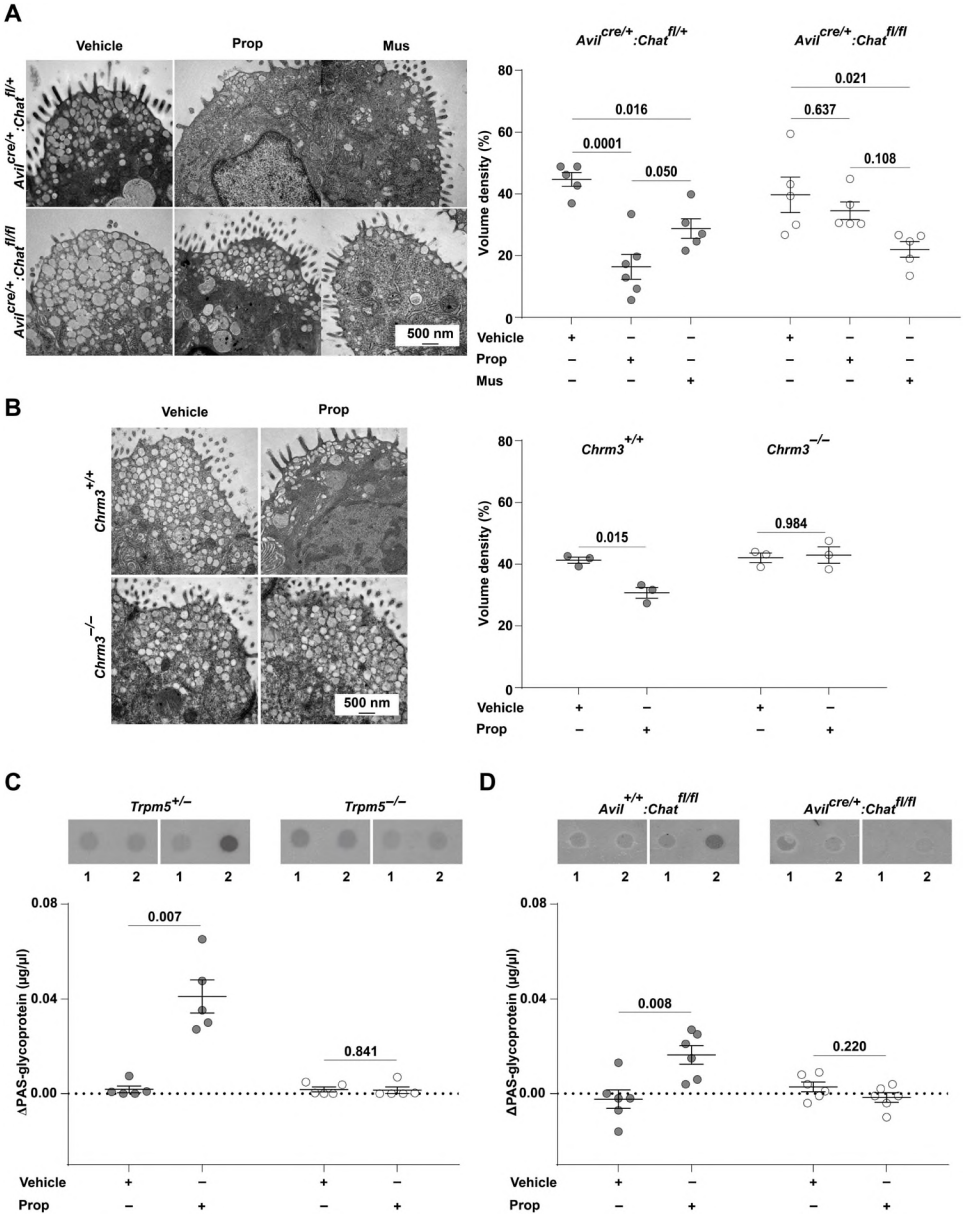

Fig. 5. Propionate triggers cholinergic tuft cell signaling to cholangiocytes. (**A** and **B**) Mucin granule volume density in the apical cytoplasm of cholangiocytes; representative ultrastructural images are shown on the left. (A) Explanted gallbladders from mice with tuft cell–specific *Chat* deletion ($Avil^{Cre}$:$Chat^{fl/fl}$) and from littermate controls ($Avil^{Cre}$:$Chat^{fl/+}$) were stimulated with vehicle, propionate (5 mM), or muscarine (10 μM); $n = 6$ for propionate stimulation of $Avil^{Cre}$:$Chat^{fl/+}$gallbladders and $n = 5$ for all other groups. ANOVA with Tukey post hoc test. (B) Explanted gallbladders from $Chrm3^{+/+}$ and $Chrm3^{-/-}$ mice were stimulated with propionate (5 mM) or vehicle ($n = 3$ for each experiment). Unpaired *t* test. (**C** and **D**) Glycoprotein released into the supernatant of explanted gallbladders quantified by densitometry of PAS-reacted dot blots. Representative dot blots depicted; full blots shown in fig. S11 (dot 1: sample taken before and dot 2: sample taken after stimulation). (C) Explanted gallbladders from $Trpm5^{+/-}$ and $Trpm5^{-/-}$ mice ($n = 5$ for each group) and from $Avil^{Cre}$:$Chat^{fl/+}$ and $Avil^{Cre}$:$Chat^{fl/fl}$ mice ($n = 6$ for each group) were stimulated with propionate (5 mM) or vehicle. Mann-Whitney test. Whiskers: means ± SEM throughout. Data are from three independent experiments in (A), (C), and (D) and from two independent experiments in (B).

Muc4 in the mouse gallbladder and additional strong expression of *Muc6*, but expression of these genes was not altered in $Pou2f3^{-/-}$ mice lacking tuft cells (fig. S13). Rather, an up-regulation was noted for *Muc2* expression, and *Muc5b* expression was detectable in $Pou2f3^{+/-}$ and $Pou2f3^{-/-}$ mice only (fig. S13). Collectively, these data showed a marked effect of tuft cell stimulation on acute mucus release, but tuft cells were not required for steady-state production of mucins reflected by mucin gene expression.

DISCUSSION

Collectively, our data identify a metabolite of intestinal bacteria, i.e., propionate, that triggers a nonredundant corelease of ACh and CysLT from gallbladder tuft cells through an FFAR2-TRPM5 signaling pathway (Fig. 6). Along this dichotomous target-specific tropism, CysLTs cause smooth muscle constriction by acting upon CysLTR1, and ACh stimulates mucin granule exocytosis via the M3R. Gallbladder motor activity and mucin secretion are mostly seen in the context of bile storage and emptying, with a focus upon the cytoprotective effect of mucins together with bicarbonate against bile acid–induced epithelial injury (*1*). In the presence of invading pathogens, however, mucins are likely to be the first molecules that these intruders interact with before they come into contact with the epithelial cells. Interaction with mucins limits binding to cellular surface glycoproteins and, thus, can neutralize the pathogen (*31*). Accordingly, increased mucus production is a long-known defense reaction of the infected gallbladder (*32*). Muscle contraction also counteracts pathogen invasion in that it flushes the contents and hampers further ascent by closing the lumen, representing a denial-of-ingress mechanism. Chemosensory cells of the urinary tract and at the opening of the vomeronasal duct into the nasal cavity also operate with such denial-of-ingress mechanisms, but there they use cholinergic signaling to sensory nerve fibers. In the urinary tract, these sentinel cells reside exclusively in the urethra, and their stimulation activates a neural reflex initiating urinary bladder contraction, i.e., micturition (*33*). In the nose, cholinergic signaling induces release of neuropeptides from capsaicin-sensitive sensory nerve fibers, and the resulting mucosal swelling occludes the entrance to the vomeronasal organ and protects it from ingression of harmful substances (*12*, *34*). In the gallbladder, however, neither previous ultrastructural studies (*2*, *29*) nor our whole-mount staining revealed a structural basis for

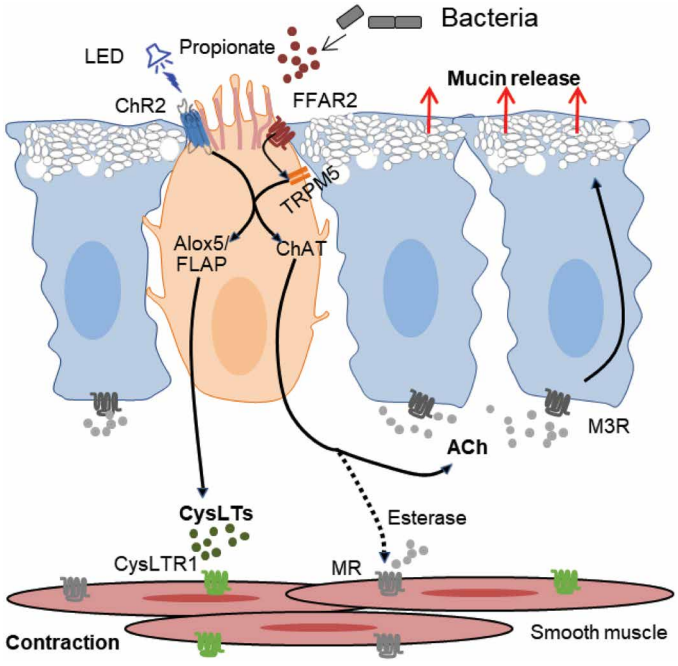

Fig. 6. Schematic of the proposed dichotomous effects of ACh and CysLTs upon gallbladder tuft cell activation. Stimulation of gallbladder tuft cells with either LED illumination in an optogenetic mouse model expressing ChR2 in tuft cells or with the bacterial metabolite, propionate, acting upon the SCFA receptor FFAR2 results in a TRPM5-dependent corelease of ACh and CysLTs into the surrounding tissue. Along this dichotomous target-specific tropism, CysLTs cause smooth muscle contraction by acting on CysLTR1, and ACh stimulates mucin granule exocytosis through epithelial M3R. Spreading of ACh to gallbladder smooth muscle is limited by local activity of cholinesterases.

tuft cell–nerve fiber interaction, and neither global activation of nerve fibers with electrical field stimulation nor selectively addressing peptidergic sensory nerve fibers with capsaicin mimicked the effects of tuft cell stimulation by propionate.

Propionate and acetate, both FFAR2 agonists, are the main physiologic products of fermentation of dietary fibers by *Bacteroides* species in the cecum and colon, where their concentration is about 100 mM (acetate:propionate about 3:1) in humans (*35*). They are taken up into the circulation and metabolized by peripheral tissues. The systemic blood concentration, however, is below the level sufficient to activate tuft cell–driven mechanisms (*35*). Thus, propionate surveillance by gallbladder tuft cells reflects local production of propionate by bacteria or reflux from the duodenum, both representing a pathological condition, rather than colonic fermentation or energy metabolism. Simple reflux of duodenal juice alone would not allow for initiating tuft cell responses, because its propionate concentrations were even lower than those found in bile, and both were below the activating threshold of tuft cells in mice kept under laboratory conditions. Duodenal propionate might vary in wild animals feeding upon naturally occurring food such as rotting grains, but actual data are not available. Yet, sphincter of Oddi laxity, the underlying cause of regurgitation of duodenal content, is commonly associated with bacterial infection, especially by Enterobacteriaceae (*36*, *37*). In inflammatory conditions, various enteropathogens, including *Salmonella* serovars and adherent-invasive *Escherichia coli*, are able to use alternate carbon sources for respiration resulting in propionate production independent of fiber fermentation. A particularly prominent source is 1,2-propanediol that derives from fermentation of fucose cleaved from mucosal glycoconjugates (*38*, *39*). Bacterial conversion of 1,2-propanediol ultimately results in formation of propionate without concomitant generation of acetate and butyrate (*40*), a profile matching the sensitivity of gallbladder tuft cells. Bile salts trigger this metabolic adaptation in adherent-invasive *E. coli* (*39*). Thus, propionate may represent a danger signal in the biliary system, monitored by an FFAR2–tuft cell defense mechanism against inadvertent ascent of gut microbiota.

MATERIALS AND METHODS

Study design

The aim of this study was to delineate the role of gallbladder tuft cells in innate defense mechanisms. Because the activating stimuli for gallbladder tuft cells were not known, we first used an optogenetic model to stimulate tuft cells of explanted mouse gallbladders directly, which allowed us to identify gallbladder contraction and mucus secretion as effector mechanisms. On the basis of previous data, we anticipated ACh and CysLTs as potential mediators of tuft cell–driven effects and addressed these hypotheses by direct measurement of their release into the medium after stimulation, localization of their synthesizing enzymes by in situ hybridization and immunohistochemistry, and use of adequate pharmacological inhibitors and genetic models in functional experiments. We then used these readouts and genetic models to screen for naturally occurring microbial products activating tuft cells and identifying crucial elements of the intracellular signaling pathway.

Mice

Mice older than 8 weeks were used throughout. Mice were age-matched within each experiment; pooled results include both male and female mice of varying ages. All animals were housed under specific pathogen–free standard laboratory conditions (10 hours dark and 14 hours light), with free access to food and water. C57BL/6JRj mice were purchased from Janvier Labs. A mouse line carrying a constitutive null mutation in *Trpm5* (*B6.129P2-Trpm5*^{tm1Dgen}/J; stock no. 005848) was obtained from the Jackson Laboratory and backcrossed (six generations) onto the C57BL/6J background. Mouse lines ChAT-ChR2-EYFP (*13*) [B6.Cg-Tg(Chat-COP4∗H134R/EYFP,Slc18a3)6Gfng/J; 014546], ChAT-EGFP (enhanced green fluorescent protein) [B6.Cg-Tg(RP23-268 L19-EGFP)2Mik/J; 007902], Chat^{fl} (B6;129-Chat^{tm1Jrs}/J; 016920), B6;129S6-*Chat*$^{tm2(cre)Lowl}$/J (stock no. 006410), B6;129-Gt(ROSA)26Sor$^{tm1(CAG-COP4*E123T*H134R,-tdTomato)Gfng}$/J (stock no. 017455), *Cysltr1*$^{-/-}$ (C57BL/6N-*Cysltr1*^{tm1Ykn}/J; stock no. 030814), and *Chrm3*$^{-/-}$ [B6N.129S6(B6J)-*Chrm3*^{tm1Jwe}/J; stock no. 030163] and wild-type (C57BL/6NJ; stock no. 005304) mice were purchased from the Jackson Laboratory. B6;129S6-*Chat*$^{tm2(cre)Lowl}$/J mice were crossed with B6;129-Gt(ROSA)26Sor$^{tm1(CAG-COP4*E123T*H134R,-tdTomato)Gfng}$/J mice, resulting in a strain expressing ChR2-tdTomato fusion protein under the control of the endogenous ChAT promoter. The following mouse strains were characterized previously: B6;D2-Tg(Avil-cre)1Phep/Cnrm (Avil-cre) mice (*41*), Pou2f3^{tm1Abek} (*Pou2f3*$^{-/-}$) (*42*), and Ffar2-mRFP and *Ffar2*$^{-/-}$ (*43*). ChAT-ChR2-EYFP and *Pou2f3*$^{-/-}$ mice were backcrossed (six generations) to the C57BL/6J background. To generate B6;129-Chat^{tm1Jrs}/J-B6;D2-Tg(Avil-Cre)1Phep/Cnrm (*Avil*^{Cre}:*Chat*$^{fl/fl}$) mice, the strains B6;129-Chat^{tm1Jrs} (*44*) and B6;D2-Tg(Avil-Cre)1Phep/Cnrm (*41*) were crossbred. As control

mice, heterozygous or homozygous wild-type littermates were used, except for data shown in Fig. 3C and fig. S7C, where C57BL/6J mice served as controls for *Trpm5*$^{-/-}$ and *Pou2f3*$^{-/-}$ mice and where C57BL/6NJ mice served as controls for *Cysltr1*$^{-/-}$ and *Chrm3*$^{-/-}$ mice. Animals were anesthetized by isoflurane (5%) (Abbott) or carbon dioxide and euthanized by transecting the inferior vena cava. All animals were handled in accordance with the guidelines established by the European Community for the care and use of animals. Breeding and use of samples of euthanized mice for further in vitro experiments were registered by the responsible authorities at the Regierungspräsidium Giessen (Hesse) and Darmstadt (Hesse), Germany (registration numbers 571_M, 572_M, 573_M, 641_M, 714_M, 717_M, 720_M, Ex-14-2018, Ex-1-2020, and 43repMMTVneu).

Immunofluorescence

Samples to be sectioned were fixed by immersion in Zamboni solution [2% paraformaldehyde (PFA)/15% saturated picric acid in 0.1 M phosphate buffer (pH 7.4)] for at least 4 hours, washed in 0.1 M phosphate buffer, and further processed for paraffin embedding and sectioning (8 μm) or cryosectioning (8 to 10 μm) as described in detail earlier (*11*) with primary and secondary antibodies listed in table S1. Sections were evaluated by epifluorescence (Olympus, BX60) or confocal laser scanning microscopy (Zeiss, LSM710).

The following controls were conducted on gallbladder sections: Antibodies directed against TRPM5 and Pou2f3 were applied to sections from respective global knockout mice and did not label cells in these preparations. The ChAT antibody labeled advillin-positive cells from wild-type but not from *Avil*$^{Cre/+}$:*Chat*$^{fl/fl}$ mice. Antibodies against fluorescent proteins GFP and mCherry/RFP did not label cells in wild-type animals. Antibodies raised in goat (against ChAT, COX1, COX2, and FLAP) were replaced by normal goat serum, resulting in no staining of epithelial cells. As positive controls, sections from taste buds of the tongue and trachea were run in parallel, revealing positive labeling of taste cells and tracheal chemosensory cells (PLCβ2, TRPM5, Pou2f3, and ChAT). A section of small intestine run in parallel revealed positive labeling of intestinal tuft cells (PLCβ2, TRPM5, Pou2f3, ChAT, COX1, COX2, and FLAP) and enteric neurons (ChAT).

For whole-mount immunostainings of gallbladders ($n = 9$), mice were transcardially perfused with buffered 4% PFA and post-fixed in the same fixative for two additional hours, and tissue clearing was done as described by Treweek *et al.* (*45*). Gallbladders were incubated overnight in 4% acrylamide at 4°C, polymerized for 3 hours at 37°C, cleared with 8% sodium dodecyl sulfate for 48 hours, and subsequently incubated overnight in 10% horse serum, 0.5% Tween 20, and 0.1% bovine serum in phosphate-buffered saline (PBS) to block nonspecific binding sites. Incubation with the primary antibodies was done for 48 hours at room temperature followed by 48 hours of incubation with the secondary antibody (table S1). The samples were mounted in HistoDenz (refractive index = 1.47) (Sigma-Aldrich) for evaluation by confocal laser scanning microscopy.

Cholinesterase histochemistry

Gallbladders were fixed in 4% PFA for 2 hours at 4°C and processed for cryosectioning (four gallbladders) or whole-mount preparations ($n = 5$). Staining for AChE and BChE activities was conducted as described and validated in *Ache*$^{-/-}$ and *Bche*$^{-/-}$ mice earlier (*46*). Specimens were examined with bright-field microscopy (Axioplan 2, Zeiss).

Electron microscopy and stereology

Gallbladders were explanted and collected in 0.3 ml of 37°C warm minimum essential medium (MEM). Gallbladders from ChAT-ChR2-EYFP and corresponding controls were opened longitudinally and incubated for either 15 min in MEM or 5 min in MEM and 10 min with atropine (1 μM, 10 min; Sigma-Aldrich, A0257) in MEM. Gallbladders were stimulated with LED for 2 min as described above, followed by 7 min additional incubation time at 37°C. Gallbladders for chemical stimulation were opened by cutting off the fundus and incubated with sodium propionate (5 mM; Sigma-Aldrich, P5436), muscarine chloride (10 μM; Sigma-Aldrich, M104), or vehicle (distilled water) for 30 min in 2 ml of 37°C warm MEM. Then, specimens were fixed in 1.5% glutardialdehyde and 2.5% PFA in 0.1 M phosphate buffer (pH 7.4) for 24 hours, washed in 0.1 M tris-HCl buffer, osmicated for 2 hours in buffered 1% OsO_4, washed (5 × 5 min) with water, stained overnight en bloc in 1% aqueous uranyl acetate, washed again (5 × 5 min) with water, dehydrated in ascending concentrations of ethanol, and embedded in EMbed 812 epoxy resin (Electron Microscopy Sciences, 14120). Sections of about 80 nm thickness (Reichert Ultracut E, Leica) were stained with alkaline lead citrate and viewed with an EM 902 transmission electron microscope (Zeiss) equipped with a 2K charge-coupled device camera (Tröndle Restlichtverstärkersysteme, Moorenweis, Germany). Only cholangiocytes that were cut along their entire apicobasal extension, i.e., facing the lumen for at least 3 μm and reaching the basal lamina, were evaluated with partial investigator blinding. Sample size (i.e., number of cholangiocytes) needed to obtain a representative value for a given specimen was determined using the equation provided by Baur (*47*), accepting a 10% change in mean value at maximum when a hypothetical additional data point would deviate from the mean by 3 SDs. On this basis, a number of 19 cholangiocytes proved to be sufficient in pilot datasets, and we chose 20 for the final evaluation. The first 20 cholangiocytes appearing in the sections and fulfilling this inclusion criterion were imaged at ×20,000 original magnification and evaluated by stereology point counting for mucin granule volume density in the uppermost 1-μm layer of cytoplasm using dot-and-line grids with 250-nm spacing. The operator taking ultrastructural images for stereological evaluation of mucin granule volume density was blinded to the genotype of animals in experiments depicted in Fig. 5A. The operator performing stereological analysis of mucin granule volume density was blinded to the genotype of animals in experiments involving cell type–specific ChAT deletion and *Chrm3* deficiency (Fig. 5, A and B). There was no blinding in other experiments.

Glycoprotein measurement

Gallbladders were explanted and collected in 0.2 ml of 37°C warm MEM. Gallbladders from *Trpm5*$^{-/-}$, *Avil-Cre*$^{tg/+}$:*Chat*$^{fl/fl}$, and C57BL/6 mice and their corresponding controls (*Trpm5*$^{+/-}$; *Avil-Cre*$^{+/+}$:*Chat*$^{fl/fl}$) were opened longitudinally, washed, and incubated for 10 min in 0.2 ml of 37°C warm MEM, and the supernatants were collected. Then, gallbladders were stimulated with sodium propionate (5 mM; Sigma-Aldrich, P5436), capsaicin (300 nM; Sigma-Aldrich, A0257), or appropriate vehicle (distilled water or ethanol) for 30 min in 0.2 ml of 37°C warm MEM. Glycoprotein in the supernatant was assessed by periodic acid–Schiff (PAS) staining of polyvinylidene fluoride (PVDF) membranes as modified from previously described methods (*48*). A total of 200 μl of the supernatants or standards were screened using a 96-well Bio-Dot Microfiltration apparatus

(Bio-Rad, Hercules, CA, 1706545), according to the manufacturer's instructions. Briefly, supernatants were blotted on PVDF membrane (Millipore, Darmstadt, Germany) and set on wet filter paper (Bio-Dot SF Filter Paper, Bio Rad). After all samples are loaded on the membrane, the apparatus was allowed to sit for a minimum of 10 min without vacuum to allow protein samples to bind. The membrane was placed on clean filter paper to dry for a minimum of 30 min. For PAS staining, after a brief distilled water rinse, the membrane was exposed to 0.5% periodic acid solution for 15 min, rinsed with distilled water, and exposed to Schiff's reagent intense (Sigma-Aldrich, 102572) for 30 min followed by two 3-min exposures to 0.6% sodium metabisulfite. After a final distilled water rinse, the membrane was dried and then digitized by a scanner (Canon CanoScan LiDE 210, Amsterdam, the Netherlands), and the optical density of the stained protein was assessed with ImageJ software and GraphPad Prism version 7. The concentration of glycoprotein in the samples was determined, referring to a standard curve of pig gastric mucus (Sigma Aldrich, M2378; range, 0.012 to 1 μg/μl).

Organ bath force recordings

Gallbladders were mounted in MEM between two stainless steel clips in an organ bath for recording of isometric tension as previously described in detail for the mouse trachea (*11*). Gallbladders were equilibrated against a passive load of 1 g, then adjusted to 0.5 g tension, and equilibrated for 30 min until they reached a stable baseline tension. Changes in tension were recorded as force in millinewtons and evaluated by appropriate software. When data are presented as Δforce in percent, the data point immediately before the first stimulus was set as reference value (100%). Chemical stimuli and inhibitors were muscarine chloride (Sigma-Aldrich, M104), CCK fragment 26-33 amide (CCK; Sigma-Aldrich, C2175), LTC4 (Cayman Chemical, 20210), *N*-methyl LTC4 (Cayman Chemical, 13390), LTD4 (Cayman Chemical, 20310), LTE4 (Cayman Chemical, 20410), sodium acetate trihydrate (Sigma-Aldrich, S8625), sodium propionate (Sigma-Aldrich, P1880), sodium butyrate (Sigma-Aldrich, B5887), and succinic acid (Sigma-Aldrich, S9512); inhibitors were atropine (1 μM; Sigma-Aldrich, A0257), MK-571 [1 μM; Sigma-Aldrich, M7571; vehicle control: dimethyl sulfoxide (DMSO) 0.001%], MK-886 (1 μM; Cayman Chemical, 10133; vehicle control: ethanol 0.001%), 3-(((3-carboxycyclohexyl)amino)carbonyl)-4-(3-(4-(4-(cyclohexyloxy) butoxy)phenyl)propoxy)benzoic acid (HAMI3379; 1 μM MedChemExpress, HY-112248; vehicle control: DMSO 0.001%), and zileuton (10 μM; Cayman Chemical, 10006967; vehicle control: DMSO 0.001%). For optogenetic stimulation, ChAT-ChR2-YFP, ChAT-ChR2-tdTomato, and corresponding control gallbladders were stimulated with LED (456 nm, 2 min, 8 Hz, and 60-ms pulse) duration using a UHP-T-DI-LED source (Prizmatix), a transistor-transistor logic pulse train generator (S/N 7276, Prizmatix), and an LED controller (ultra high power LED current controller, Prizmatix) controlled by Prizmatix Pulser software. At the end of each experiment, CCK (0.1 μM) and/or LTD4 (0.1 μM) was applied as a vitality control. Only those gallbladders showing an increase in tension of at least 20% in response to this final test stimulus were included in the study.

ACh measurement by HPLC

Gallbladders from ChAT-ChR2-EYFP and corresponding control mice were dissected, freed from surrounding tissue, placed in a glass dish covered with Sylgard polymer, and fixed on silicon elastomer with needles. The gallbladder was cut longitudinally and rinsed in 0.3 ml of 37°C warm MEM (Gibco, 51200038) supplemented with 10 μM eserine (Sigma-Aldrich, E-805) and 1% penicillin/streptomycin (Sigma-Aldrich, P4333) for 5 min before the first supernatant was collected. Then, gallbladders were stimulated with blue LED light (456 nm, 2 min, 8 Hz, and 60-ms pulse duration), and the second supernatant was collected after an additional 5 min. Supernatants were snap-frozen in liquid nitrogen and stored at −80°C until further use for ACh measurement by high-performance liquid chromatography (HPLC) as previously described (*11*).

Prostanoid and leukotriene measurement

Gallbladders were dissected, opened longitudinally, incubated in 0.3 ml of MEM (5 min), stimulated with LED (456 nm, 8 Hz, 2 min), and kept at 37°C for a further 5 min. The supernatants before and after stimulation were collected, frozen immediately, and kept at −80°C until further analysis. Prostanoids were measured as described previously (*49*); i.e., 100 μl of supernatant was spiked with isotopically labeled internal standards [prostaglandin (PG)D2-d4, thromboxane (TX)B2-d4, PGF2α-d4, and 6-keto PGF1α-d4] before liquid-liquid extraction using ethyl acetate. The liquid chromatography–tandem mass spectrometry (LC-MS/MS) analysis was carried out using an Agilent 1290 Infinity LC system (Agilent) coupled to a hybrid triple quadrupole linear ion trap mass spectrometer QTRAP 6500+ (Sciex) equipped with a Turbo V source operating in negative electrospray ionization mode. The chromatographic separation was carried out using a Synergi Hydro-RP column (150 × 2 mm, 4-μm particle size, and 80-Å pore size; Phenomenex) under gradient conditions with water and acetonitrile as mobile phases, both containing 0.0025% formic acid. For the analysis and quantification, Analyst software 1.6 and MultiQuant software 3.0.2 (Sciex) were used, using the internal standard method (isotope dilution MS). The analysis of hydroxy-eicosatetraenoic acid (HETE) and leukotriene (LT)B4 was done as described previously (*50*). In brief, 100 μl of supernatants was spiked with the corresponding deuterated internal standards and extracted by liquid-liquid extraction using ethyl acetate. Analytics were separated using a Gemini NX C18 RP-LC column (150 mm × 2 mm internal diameter, 5-μm particle size, and 110-Å pore size; Phenomenex) under gradient conditions with water and acetonitrile as mobile phases, both containing 0.01% ammonia solution. The LC system was coupled to a mass spectrometer QTRAP 5500 (Sciex) equipped with a Turbo V source operating in negative electrospray ionization mode. Data acquisition was done using Analyst software V 1.6, and quantification was performed with MultiQuant software V 3.0.2 (Sciex) using the internal standard method (isotope dilution MS). Levels of CysLTs were measured with the commercially available LTC4/D4/E4 ELISA kit (Enzo Life Sciences, ADI-900-070) according to the manufacturer's instruction. The Δ% indicates the prostanoid or leukotriene content presented in 5 min after stimulation compared with baseline level (the value before stimulus application).

SCFA analysis

Samples were derivatized with the AMP^+ MaxSpec Kit (Cayman Chemical, Ann Arbor, USA, 710000) according to the manufacturer's instructions. Briefly, the samples were derivatized by adding 20 μl of acetonitrile/dimethylformamide, 20 μl of 1-ethyl-3-(3-dimethylaminopropyl)carbodiimide, 10 μl of 1-hydroxybenzotriazole (Sigma-Aldrich), and 30 μl of the AMP^+ reagent. The reaction mixture was incubated for 30 min at 60°C. Samples were stored at −20°C before analysis. AMP^+-derivatized SCFAs were separated on

a Hypercarb column (3 μm, 100 × 2.1 mm; Thermo Fisher Scientific, 35003-031030) using a gradient of solvent A (5% acetonitrile and 0.1% formic acid) and solvent B (100% acetonitrile). After 5 min of 100% solvent A, the proportion of solvent B was increased to 100% within 15 min at a flow rate of 200 μl/min at 30°C. Quantification of SCFA was performed by LC-ESI-MS (Alliance HT Waters 2790 with Waters Micromass ZQ 4000, Waters, Eschborn, Germany, 176004001) using the selected ion recording mode for the AMP^+ signals 227 (acetic acid), 241 (propionic acid), 255 (butyric acid), and 269 (valeric acid) (Sigma-Aldrich). For absolute quantification, an SCFA standard calibration mixture (WSFA-2; Merck, Darmstadt, Germany, 46975-U) was used.

RT-PCR and real-time PCR

For qualitative expression analysis of *Cox1*, *Cox2*, *Cysltr1*, and *Cysltr2*, gallbladder and colon (positive control) were obtained from four C57BL/6J mice. The samples were shock-frozen in RLT plus lysis buffer (QIAamp DNA Mini Kit, QIAGEN, 51304) and stored at −80°C until use. The total RNA was isolated by using the RNeasy method according to the manufacturer's protocol (QIAGEN). Contaminating DNA was degraded using 1 U deoxyribonuclease (DNase) I (Invitrogen) per microgram of total RNA, and reverse transcription (RT) was done for 50 min at 42°C using 200 U Superscript II reverse transcriptase (Invitrogen, 18064014) per microgram of RNA. RT–polymerase chain reaction (PCR) was performed by adding 1 μl of cDNA, 0.3 μl of each primer, 2.5 μl of 10× PCR buffer II [100 mM tris-HCl and 500 mM KCl (pH 8.3)], 2 μl of $MgCl_2$ (15 mM), 0.6 μl of deoxynucleotide triphosphate (10 mM each), 0.15 μl of AmpliTaq Gold polymerase (5 U/μl; all reagents from Applied Biosystems), and 18.15 μl of H_2O. PCR primers are specified in table S2. Cycling conditions were 5 min at 94°C, 40 cycles with 20 s at 94°C, 20 s at 60°C, 20 s at 73°C, and a final extension at 72°C for 7 min. Control reactions included the absence of DNA template and the absence of reverse transcriptase. A 100–base pair (bp) DNA ladder (Invitrogen, 15628050) was run as marker (6.5 μl). The PCR products were separated by electrophoresis on a 2% tris-acetate EDTA agarose gel and detected by ultraviolet illumination (Biochrom Ultrospec, 2100 Pro).

Real-time PCR (iCycler, Bio-Rad, Germany; iTaq Universal SYBR Green Supermix, Bio-Rad Laboratories Inc., CA, USA) was conducted on gallbladders and tongues from nine C57BL/6J and six $Pou2f3^{-/-}$ mice to quantify *Trpm5* expression and on gallbladders from $Pou2f3^{+/+}$, $Pou2f3^{+/-}$, and $Pou2f3^{-/-}$ mice (*n* specified in respective figure legends) to quantify *Mcpt1*, *C-kit*, *Ly6g*, and mucin gene expression, with cDNA obtained as described above. PCR primers are specified in table S2. The PCR conditions included initial denaturation for 10 min at 95°C followed by 45 cycles of 30 s at 95°C, 30 s at 61°C, and 30 s at 72°C for *Trpm5*, and initial denaturation for 3 min at 95°C followed by 45 cycles of 15 s at 95°C, 15 s at 61°C, and 15 s at 72°C for the other targets. Relative expression was calculated as $2^{-\Delta CT}$, with CT = cycle threshold and ΔCT = CT (*target*) − CT (*B2m*).

In situ hybridization

For gene expression analyses on tissue sections, gallbladders ($n = 5$) were placed in Tissue-Tek compound and quickly frozen in isopentane. After an initial storage at −70°C, 16-μm-thick tissue sections were cut, mounted on silanized glass slides, and subjected to an established in situ hybridization protocol (*40*). The generation of a template for the detection of *Egfp* transcripts has been described previously (*5*). DNA fragments from *Trpm5* (GenBank accession no. NM_020277.2, nucleotides 461 to 1293, 832 bp), *Cox1* (GenBank accession no. NM_008969.4, nucleotides 1060 to 1915, 856 bp), *Cox2* (GenBank accession no. NM_011198.4, nucleotides 1114 to 1947, 834 bp), *Alox5* (GenBank accession no. NM_009662.2, nucleotides 821 to 1586, 766 bp), and *Ltc4s* (GenBank accession no. NM_008521.2, nucleotides 31 to 606, 576 bp) were amplified by PCR from mouse C57BL/6J ileum cDNA and subcloned into pGEM-T (Promega), and the inserted sequence was confirmed by double-stranded sequencing and used as templates for the generation of digoxygenin-labeled (*Egfp*) or ^{35}S-labeled (all others) riboprobes.

Flow cytometry

Flow cytometry analyses were performed exactly as described before (*51*). $Pou2f3^{+/+}$, $Pou2f3^{+/-}$, and $Pou2f3^{-/-}$ mice were euthanized and immediately perfused via the heart with 10 ml of cold PBS (Gibco, Darmstadt, Germany). Gallbladders and kidneys were cut into small pieces and digested in RPMI 1640 medium containing collagenase A (1 mg/ml; Roche, Munich, Germany) and DNase I (0.05 mg/ml; Roche) at 37°C in shaking water bath. Digested material was passed four to five times through a 3-ml syringe attached with a 21-G needle and filtered through a 70-μm filter. The cells were centrifuged (350*g* for 5 min at 4°C), and red blood cells were lysed in red blood cell lysis buffer (QIAGEN). The cells were suspended in fluorescence-activated cell sorting (FACS) buffer (PBS containing 2% fetal calf serum; Gibco) and 2 mM EDTA (Sigma-Aldrich) and incubated with Fc blocker (1:10 dilution; Miltenyi Biotec, Bergisch Gladbach, Germany) for 10 min before staining with antibodies (table S3) for 30 min at 4°C. After staining, cells were washed and dissolved in FACS buffer. Flow cytometry analysis was performed using a MACSQuant Analyzer 10 flow cytometer (Miltenyi Biotec), and data were analyzed with the FlowJo software version X (Tree Star, Ashland, OR, USA).

Statistical analysis

All experiments were performed using randomly assigned mice. All data points and "*n*" values reflect biological replicates (i.e., mice). Reproducibility was verified by replicating experiments as specified in the respective figure legends. All experimental findings described here were reliably reproduced as seen in the scatterplots depicting all individual data points and means ± SEM. Data in the graphs depicting time courses or dose responses are presented as means ± SEM. No data were excluded, except experimental samples that did not respond to the viability controls at the end of the experiment (see the "Organ bath force recordings" section). Statistical analysis was performed as noted in figure captions using Prism 7 (GraphPad software). An assessment of the normality of the data was done using the Kolmogorov-Smirnov normality test. Data on ACh release and mucin granule volume densities were evaluated by unpaired *t* test or analysis of variance (ANOVA) with post hoc Tukey correction. All other data were analyzed by nonparametric tests (Mann-Whitney *U* test or Kruskal-Wallis test followed by Dunn's multiple comparisons test). The values for maximal efficacy (E_{max}) and EC_{50} were estimated using nonlinear regression sigmoidal curve analysis according to the Hill equation. No statistical methods were used to predetermine the sample size, except for stereology on cholangiocytes as described above. Differences were considered as statistically significant when $P \leq 0.05$.

SUPPLEMENTARY MATERIALS

www.science.org/doi/10.1126/sciimmunol.abf6734
Figs. S1 to S13
Tables S1 to S3
Data file S1
MDAR Reproducibility Checklist

View/request a protocol for this paper from *Bio-protocol*.

REFERENCES AND NOTES

1. C. Housset, Y. Chretien, D. Debray, N. Chignard, Functions of the gallbladder. *Compr. Physiol.* **6**, 1549–1577 (2016).
2. L. Luciano, Fine structure of gallbladder and biliary ducts. I. The epithelium of the mouse gallbladder. *Z. Zellforsch. Mikrosk. Anat.* **135**, 87–102 (1972).
3. H. A. Ting, J. von Moltke, The immune function of tuft cells at gut mucosal surfaces and beyond. *J. Immunol.* **202**, 1321–1329 (2019).
4. S. Kaske, G. Krasteva, P. König, W. Kummer, T. Hofmann, T. Gudermann, V. Chubanov, TRPM5, a taste-signaling transient receptor potential ion-channel, is a ubiquitous signaling component in chemosensory cells. *BMC Neurosci.* **8**, 49 (2007).
5. B. Schütz, I. Jurastow, S. Bader, C. Ringer, J. von Engelhardt, V. Chubanov, T. Gudermann, M. Diener, W. Kummer, G. Krasteva-Christ, E. Weihe, Chemical coding and chemosensory properties of cholinergic brush cells in the mouse gastrointestinal and biliary tract. *Front. Physiol.* **6**, 87 (2015).
6. M. S. Nadjsombati, J. W. Mc Ginty, M. R. Lyons-Cohen, J. B. Jaffe, L. D. Peso, C. Schneider, C. N. Miller, J. L. Pollack, G. A. N. Gowda, M. F. Fontana, D. J. Erle, M. S. Anderson, R. M. Locksley, D. Raftery, J. von Moltke, Detection of succinate by intestinal tuft cells triggers a type 2 innate immune circuit. *Immunity* **49**, 33-41.e37 (2018).
7. C. Schneider, C. E. O'Leary, R. M. Locksley, Regulation of immune responses by tuft cells. *Nat. Rev. Immunol.* **19**, 584–593 (2019).
8. F. Gerbe, E. Sidot, D. J. Smyth, M. Ohmoto, I. Matsumoto, V. Dardalhon, P. Cesses, L. Garnier, M. Pouzolles, B. Brulin, M. Bruschi, Y. Harcus, V. S. Zimmermann, N. Taylor, R. M. Maizels, P. Jay, Intestinal epithelial tuft cells initiate type 2 mucosal immunity to helminth parasites. *Nature* **529**, 226–230 (2016).
9. J. W. McGinty, H.-A. Ting, T. E. Billipp, M. S. Nadjsombati, D. M. Khan, N. A. Barrett, H.-E. Liang, I. Matsumoto, J. von Moltke, Tuft-cell-derived leukotrienes drive rapid anti-helminth immunity in the small intestine but are dispensable for anti-protist immunity. *Immunity* **52**, 528-541.e527 (2020).
10. C. Fung, M. R. Howitt, A tuft act to follow: Leukotrienes take the stage in anti-worm immunity. *Immunity* **52**, 426–428 (2020).
11. A. Perniss, S. Liu, B. Boonen, M. Keshavarz, A.-L. Ruppert, T. Timm, U. Pfeil, A. Soultanova, S. Kusumakshi, L. Delventhal, Ö. Aydin, M. Pyrski, K. Deckmann, T. Hain, N. Schmidt, C. Ewers, A. Günther, G. Lochnit, W. Kummer, Chemosensory cell-derived acetylcholine drives tracheal mucociliary clearance in response to virulence-associated formyl peptides. *Immunity* **52**, 683-699.e611 (2020).
12. C. J. Saunders, M. Christensen, T. E. Finger, M. Tizzano, Cholinergic neurotransmission links solitary chemosensory cells to nasal inflammation. *Proc. Natl. Acad. Sci. U.S.A.* **111**, 6075–6080 (2014).
13. S. Zhao, J. T. Ting, H. E. Atallah, L. Qiu, J. Tan, B. Gloss, G. J. Augustine, K. Deisseroth, M. Luo, A. M. Graybiel, G. Feng, Cell type-specific channelrhodopsin-2 transgenic mice for optogenetic dissection of neural circuitry function. *Nat. Methods* **8**, 745–752 (2011).
14. T. Yamaguchi, J. Yamashita, M. Ohmoto, I. Aoudé, T. Ogura, W. Luo, A. A. Bachmanov, W. Lin, I. Matsumoto, J. Hirota, Skn-1a/Pou2f3 is required for the generation of Trpm5-expressing microvillous cells in the mouse main olfactory epithelium. *BMC Neurosci.* **15**, 13 (2014).
15. H. Axelsson, A. Danielsson, R. Henriksson, T. Wahlin, Secretory behavior and ultrastructural changes in mouse gallbladder principal cells after stimulation with cholinergic and adrenergic drugs. A morphometric study. *Gastroenterology* **76**, 335–340 (1979).
16. P. W. Stengel, M. L. Cohen, Muscarinic receptor knockout mice: Role of muscarinic acetylcholine receptors M(2), M(3), and M(4) in carbamylcholine-induced gallbladder contractility. *J. Pharmacol. Exp. Ther.* **301**, 643–650 (2002).
17. M. Yoshida, T. Koeda, Studies on the electrical stimulation-induced contractile responses of hamster and mouse gallbladders. *J. Smooth Muscle Res.* **28**, 111–120 (1992).
18. P. Yusko, R. A. Hall, A. W. Ford-Hutchinson, Contraction of guinea pig gallbladder strips by leukotrienes and other agonists. *Prostaglandins* **25**, 397–403 (1983).
19. B. Schütz, A.-L. Ruppert, O. Strobel, M. Lazarus, Y. Urade, M. W. Büchler, E. Weihe, Distribution pattern and molecular signature of cholinergic tuft cells in human gastro-intestinal and pancreatic-biliary tract. *Sci. Rep.* **9**, 17466 (2019).
20. C. Bezençon, A. Fürholz, F. Raymond, R. Mansourian, S. Métairon, J. Le Coutre, S. Damak, Murine intestinal cells expressing Trpm5 are mostly brush cells and express markers of neuronal and inflammatory cells. *J. Comp. Neurol.* **509**, 514–525 (2008).
21. S. Ualiyeva, N. Hallen, Y. Kanaoka, C. Ledderose, I. Matsumoto, W. G. Junger, N. A. Barrett, L. G. Bankova, Airway brush cells generate cysteinyl leukotrienes through the ATP sensor P2Y2. *Sci. Immunol.* **5**, (2020).
22. R. A. Dixon, R. E. Diehl, E. Opas, E. Rands, P. J. Vickers, J. F. Evans, J. W. Gillard, D. K. Miller, Requirement of a 5-lipoxygenase-activating protein for leukotriene synthesis. *Nature* **343**, 282–284 (1990).
23. M. Back, W. S. Powell, S.-E. Dahlén, J. M. Drazen, J. F. Evans, C. N. Serhan, T. Shimizu, T. Yokomizo, G. E. Rovati, Update on leukotriene, lipoxin and oxoeicosanoid receptors: IUPHAR Review 7. *Br. J. Pharmacol.* **171**, 3551–3574 (2014).
24. P. Louis, H. J. Flint, Formation of propionate and butyrate by the human colonic microbiota. *Environ. Microbiol.* **19**, 29–41 (2017).
25. A. J. Brown, S. M. Goldsworthy, A. A. Barnes, M. M. Eilert, L. Tcheang, D. Daniels, A. I. Muir, M. J. Wigglesworth, I. Kinghorn, N. J. Fraser, N. B. Pike, J. C. Strum, K. M. Steplewski, P. R. Murdock, J. C. Holder, F. H. Marshall, P. G. Szekeres, S. Wilson, D. M. Ignar, S. M. Foord, A. Wise, S. J. Dowell, The Orphan G protein-coupled receptors GPR41 and GPR43 are activated by propionate and other short chain carboxylic acids. *J. Biol. Chem.* **278**, 11312–11319 (2003).
26. E. Le Poul, C. Loison, S. Struyf, J.-Y. Springael, V. Lannoy, M.-E. Decobecq, S. Brezillon, V. Dupriez, G. Vassart, J. Van Damme, M. Parmentier, M. Detheux, Functional characterization of human receptors for short chain fatty acids and their role in polymorphonuclear cell activation. *J. Biol. Chem.* **278**, 25481–25489 (2003).
27. W. R. Russell, L. Hoyles, H. J. Flint, M. E. Dumas, Colonic bacterial metabolites and human health. *Curr. Opin. Microbiol.* **16**, 246–254 (2013).
28. W. Lei, W. Ren, M. Ohmoto, J. F. Urban Jr., I. Matsumoto, R. F. Margolskee, P. Jiang, Activation of intestinal tuft cell-expressed Sucnr1 triggers type 2 immunity in the mouse small intestine. *Proc. Natl. Acad. Sci. U.S.A.* **115**, 5552–5557 (2018).
29. T. J. Nevalainen, Ultrastructural characteristics of tuft cells in mouse gallbladder epithelium. *Acta Anat. (Basel)* **98**, 210–220 (1977).
30. H. H. Wang, N. H. Afdhal, S. J. Gendler, D. Q. Wang, Targeted disruption of the murine mucin gene 1 decreases susceptibility to cholesterol gallstone formation. *J. Lipid Res.* **45**, 438–447 (2004).
31. J. J. Kim, W. I. Khan, Goblet cells and mucins: Role in innate defense in enteric infections. *Pathogens* **2**, 55–70 (2013).
32. R. H. Gilman, C. Young, R. Bulger, R. B. Hornick, B. Greenberg, Anatomical and immunological responses of rabbit gallbladders to bacterial infections. *Infect. Immun.* **36**, 407–416 (1982).
33. K. Deckmann, K. Filipski, G. Krasteva-Christ, M. Fronius, M. Althaus, A. Rafiq, T. Papadakis, L. Renno, I. Jurastow, L. Wessels, M. Wolff, B. Schutz, E. Weihe, V. Chubanov, T. Gudermann, J. Klein, T. Bschleipfer, W. Kummer, Bitter triggers acetylcholine release from polymodal urethral chemosensory cells and bladder reflexes. *Proc. Natl. Acad. Sci. U.S.A.* **111**, 8287–8292 (2014).
34. T. Ogura, K. Krosnowski, L. Zhang, M. Bekkerman, W. Lin, Chemoreception regulates chemical access to mouse vomeronasal organ: Role of solitary chemosensory cells. *PLOS ONE* **5**, e11924 (2010).
35. J. H. Cummings, E. W. Pomare, W. J. Branch, C. P. Naylor, G. T. Macfarlane, Short chain fatty acids in human large intestine, portal, hepatic and venous blood. *Gut* **28**, 1221–1227 (1987).
36. T. Liang, W. Su, Q. Zhang, G. Li, S. Gao, J. Lou, Y. Zhang, T. Ma, X. Bai, Roles of sphincter of oddi laxity in bile duct microenvironment in patients with cholangiolithiasis: From the perspective of the microbiome and metabolome. *J. Am. Coll. Surg.* **222**, 269-280.e210 (2016).
37. Q. Zhang, M. Ye, W. Su, Y. Chen, Y. Lou, J. Yang, T. Ma, W. Chen, S. Gao, R. Que, B. Zhang, H. Li, X. Bai, T. Liang, Sphincter of Oddi laxity alters bile duct microbiota and contributes to the recurrence of choledocholithiasis. *Ann. Transl. Med.* **8**, 1383 (2020).
38. F. Faber, P. Thiennimitr, L. Spiga, M. X. Byndloss, Y. Litvak, S. Lawhon, H. L. Andrews-Polymenis, S. E. Winter, A. J. Bäumler, Respiration of microbiota-derived 1,2-propanediol drives salmonella expansion during colitis. *PLOS Pathog.* **13**, e1006129 (2017).
39. J. Delmas, L. Gibold, T. Faïs, S. Batista, M. Leremboure, C. Sinel, E. Vazeille, V. Cattoir, A. Buisson, N. Barnich, G. Dalmasso, R. Bonnet, Metabolic adaptation of adherent-invasive *Escherichia coli* to exposure to bile salts. *Sci. Rep.* **9**, 2175 (2019).
40. M. Viladomiu, M. L. Metz, S. F. Lima, W.-B. Jin, L. Chou; JRI Live Cell Bank, C.-J. Guo, G. E. Diehl, K. W. Simpson, E. J. Scherl, R. S. Longman, Adherent-invasive *E. coli* metabolism of propanediol in Crohn's disease regulates phagocytes to drive intestinal inflammation. *Cell Host Microbe.* **29**, 607-619.e608 (2021).
41. S. Zurborg, A. Piszczek, C. Martínez, P. Hublitz, M. A. Banchaabouchi, P. Moreira, E. Perlas, P. A. Heppenstall, Generation and characterization of an Advillin-Cre driver mouse line. *Mol. Pain* **7**, 1744-8069-7-66 (2011).
42. I. Matsumoto, M. Ohmoto, M. Narukawa, Y. Yoshihara, K. Abe, Skn-1a (Pou2f3) specifies taste receptor cell lineage. *Nat. Neurosci.* **14**, 685–687 (2011).
43. C. Tang, K. Ahmed, A. Gille, S. Lu, H. J. Gröne, S. Tunaru, S. Offermanns, Loss of FFA2 and FFA3 increases insulin secretion and improves glucose tolerance in type 2 diabetes. *Nat. Med.* **21**, 173–177 (2015).

44. T. Misgeld, R. W. Burgess, R. M. Lewis, J. M. Cunningham, J. W. Lichtman, J. R. Sanes, Roles of neurotransmitter in synapse formation: Development of neuromuscular junctions lacking choline acetyltransferase. *Neuron* **36**, 635–648 (2002).
45. J. B. Treweek, K. Y. Chan, N. C. Flytzanis, B. Yang, B. E. Deverman, A. Greenbaum, A. Lignell, C. Xiao, L. Cai, M. S. Ladinsky, P. J. Bjorkman, C. C. Fowlkes, V. Gradinaru, Whole-body tissue stabilization and selective extractions via tissue-hydrogel hybrids for high-resolution intact circuit mapping and phenotyping. *Nat. Protoc.* **10**, 1860–1896 (2015).
46. C. Nassenstein, S. Wiegand, K. S. Lips, G. Li, J. Klein, W. Kummer, Cholinergic activation of the murine trachealis muscle via non-vesicular acetylcholine release involving low-affinity choline transporters. *Int. Immunopharmacol.* **29**, 173–180 (2015).
47. R. Baur, On estimation of the smallest permissible random sample size for stereologic measurements on histologic sections. *Experientia* **25**, 554–555 (1969).
48. Y. Akiba, P. H. Guth, E. Engel, I. Nastaskin, J. D. Kaunitz, Dynamic regulation of mucus gel thickness in rat duodenum. *Am. J. Physiol. Gastrointest. Liver Physiol.* **279**, G437–G447 (2000).
49. N. Tarighi, D. Menger, S. Pierre, L. Kornstädt, D. Thomas, N. Ferreirós, R. M. Nüsing, G. Geisslinger, K. Scholich, Thromboxane-induced α-CGRP release from peripheral neurons is an essential positive feedback loop in capsaicin-induced neurogenic inflammation. *J. Invest. Dermatol.* **139**, 656–664 (2019).
50. K. Kern, S. Pierre, Y. Schreiber, C. Angioni, D. Thomas, N. Ferreirós, G. Geisslinger, K. Scholich, CD200 selectively upregulates prostaglandin E2 and D2 synthesis in LPS-treated bone marrow-derived macrophages. *Prostaglandins Other Lipid Mediat.* **133**, 53–59 (2017).
51. M. Wang, Y. Yang, D. Cansever, Y. Wang, C. Kantores, S. Messiaen, D. Moison, G. Livera, S. Chakarov, T. Weinberger, C. Stremmel, M. Fijak, B. Klein, C. Pleuger, Z. Lian, W. Ma, Q. Liu, K. Klee, K. Händler, T. Ulas, A. Schlitzer, J. L. Schultze, B. Becher, M. Greter, Z. Liu, F. Ginhoux, S. Epelman, C. Schulz, A. Meinhardt, S. Bhushan, Two populations of self-maintaining monocyte-independent macrophages exist in adult epididymis and testis. *Proc. Natl. Acad. Sci. U.S.A.* **118**, e2013686117 (2021).

Acknowledgments: We thank A. Baumtrog, M. Bodenbenner, A. Soultanova (Giessen), and H. Lau (Frankfurt) for technical support; A. Weiss (Giessen) for access to the ELISA reader; and I. Matsumoto (Monell Chemical Senses Center, Philadelphia, PA, USA; *Pou2f3*^{tm1Abek}) and J. Siemens (Institute for Pharmacology, Ruprecht Karl University, Heidelberg, Germany; Avil-Cre) for providing mice. **Funding:** This research was funded by the German Research Foundation (grant KU 688/8-1 to W.K., grant SCHU1259/10-1 to B.S., grant BH 93/1-4 to S.B., and grants SFB-TR152 and RTG2338 to T.G. and V.C.). **Author contributions:** M.K., S.F.T., A.-L.R., U.P., Y.S., G.L., S.B., A.P., K.D., P.H., M.M., P.M., S.W., and T.P. generated data. M.K., S.F.T., A.-L.R., U.P., J.K., G.L., S.B., A.P., K.D., P.H., D.T., C.A., U.G., B.S., and W.K. analyzed data. I.B., A.R., J.O., V.C., T.G., S.O., and B.S. designed, generated, and characterized mouse models. M.K., B.S., and W.K. designed the study and wrote the initial draft of the manuscript. **Competing interests:** The authors declare that they have no competing interests. **Data and materials availability:** All data needed to evaluate the conclusions in the paper are present in the paper or the Supplementary Materials.